Nonequilibrium Fluctuation Relation for Sheared Micellar Gel in a Jammed State

Sayantan Majumdar and A. K. Sood*

Department of Physics, Indian Institute of Science, Bangalore 560012, India

(Received 14 February 2008; published 15 August 2008)

We show that the shear rate at a fixed shear stress in a micellar gel in a jammed state exhibits large fluctuations, showing positive and negative values, with the mean shear rate being positive. The resulting probability distribution functions of the global power flux to the system vary from Gaussian to non-Gaussian, depending on the driving stress, and in all cases show similar symmetry properties as predicted by the Gallavotti-Cohen steady state fluctuation relation. The fluctuation relation allows us to determine an effective temperature related to the structural constraints of the jammed state. We have measured the stress dependence of the effective temperature. Further, experiments reveal that the effective temperature and the standard deviation of the shear-rate fluctuations increase with the decrease of the system size.

DOI: 10.1103/PhysRevLett.101.078301 PACS numbers: 82.70.Uv, 05.40.−a, 05.70.Ln

For a system driven arbitrarily far from equilibrium by a large perturbation, the traditional linear response theory and the fluctuation dissipation theorem do not apply. However, remarkably strong fluctuation theorems (FTs) have been obtained for a variety of driven systems arbitrarily far from equilibrium. Motivated by the molecular dynamics simulation results on sheared hard disks in two dimensions [1], Evans and Searles derived a FT for systems going from an equilibrium to a nonequilibrium steady state [2], and Gallavotti and Cohen derived a FT for nonequilibrium stationary state systems [3]. The Gallavotti- Cohen steady state fluctuation relation (SSFR) based on chaotic hypothesis says [3]

$$Lt_{\tau\to\infty} P(+s_\tau)/P(-s_\tau) = e^{\Sigma\tau s_\tau}, \tag{1}$$

with $\Sigma = 1$. Here $s_\tau = \frac{1}{\tau}\int_t^{t+\tau} s(t')dt'$, and $s(t)$ is the rate of entropy production in the nonequilibrium steady state. $P(+s_\tau)$ is the probability of observing a fluctuation of magnitude s_τ over a phase space trajectory of duration τ, which is larger than any microscopic time scale of the system. Naturally, $P(-s_\tau)$ gives the probability of a transient violation of the second law of thermodynamics for the time τ, as the entropy decreases over this time. The physical implication of Eq. (1) is that, if the value of s_τ and τ is large, as in the case of macroscopic systems and time scales, $P(+s_\tau) \gg P(-s_\tau)$; i.e., the probability of observing entropy-increasing fluctuations is overwhelmingly large compared to those in which entropy decreases. Thus, in classical thermodynamics we never see the decrease in entropy in any physical process. Extension of the steady state fluctuation theorem for finite times is discussed in Ref. [4].

The experiments on the fluctuation relation (FR) reported so far can be broadly divided into two classes. Experiments on systems with a small number of degrees of freedom include dragging of a Brownian particle in an optical trap [5,6], electrical circuits [7], and RNA stretching [8,9], where RNA free energy between folded and unfolded states was estimated using Crook's relation and Jarzynski equality and stochastic harmonic oscillators [10,11]. The second class of experiments, which is of relevance here, includes macroscopic systems with a large number of degrees of freedom such as Rayleigh-Benard convection [12,13], pressure fluctuations on a surface kept in turbulent flows [14], vertically shaken granular beads [15], Lagrangian turbulence on a free surface [16], and liquid crystal electroconvection [17]. To our knowledge, no experimental evidence exists for the FR in large volume sheared fluids. In this Letter, we address, for the first time, an instance of the FR in the case of a macroscopic-sized sheared micellar gel in a jammed state. In our context, $s(t) = \frac{P(t)}{k_B T_{\text{eff}}}$, where $P(t)$ is the instantaneous power flux into the system and T_{eff} is the effective temperature of the system. We show that the nature of probability distribution functions (PDFs) of global power flux for the same system can be Gaussian or non-Gaussian, depending on the applied stress [18]. Further, the PDFs show similar symmetry properties as predicted in Eq. (1), even in nontrivial cases where PDFs show large deviation from the Gaussian nature. An important point is that, in our sheared system, the dominant noise is not thermal but rather athermal; i.e., it arises in the very process of driving, as in Ref. [15]. Our results also provide a method to estimate the effective temperature T_{eff} of the driven jammed state, like in the macroscopic granular system [15]. It should be emphasized that T_{eff} is an effective structural temperature estimated from the nonequilibrium fluctuations resulting from the applied stress and has nothing to do with the actual temperature of the system. We will show that T_{eff} increases with the increasing driving stress as well as decreasing system size. This result may have important significance in the statistical formulation of driven complex systems.

Our experiments are carried out on a surfactant cetyltrimethylammonium tosylate (CTAT) water system in the concentration range 35–41 wt% [19], where a hexagonal phase of surfactant cylindrical micelles is formed. The

samples are prepared by dissolving a known amount of CTAT (Sigma Aldrich) in double-distilled water and are kept for equilibration for a week at 60 °C. All of the experiments are carried out at 30 °C using a MCR 300 stress-controlled rheometer (Anton Paar, Germany) which has a minimum angular resolution of 0.01 μrad. A humidity chamber is used to minimize the evaporation of water from the sample during the rheology experiments. We have used cone and plate (CP) and parallel plate (PP) geometries with the rheometer. For both of them, the bottom plate is fixed, and the top plate (cone with angle 1.99° in the case of CP) rotates to apply shear on the sample kept between the plates. For CP the sample volume is 1.3×10^{-7} m^3, and for PP the sample volume was varied between 0.98×10^{-7} and 0.49×10^{-8} m^3 as the gap is changed from 200 to 10 μm, respectively. The results presented in Figs. 1 and 2 are done in CP, and the system size dependence (Fig. 3) is done in PP. The sample is subjected to a constant shear stress (σ), and the shear rate ($\dot{\gamma}$) is measured as a function of time. The time resolution is 40 ms between two consecutive data points in the shear-rate measurements. The shear rate shows interesting time dependence, which is known as "aging" and "shear rejuvenation" [20]. Here, below a critical shear stress, the shear rate decreases with time (i.e., viscosity increases with time, known as aging) as shown in Fig. 1(a), whereas, at higher stresses, the viscosity decreases with time (known as rejuvenation, which is not shown in Fig. 1). To characterize the jammed state, we carried out a stress sweep on the sample [Fig. 1(c)] with a waiting time of 20 s for each data point, after the steady jammed state is fully reached [Fig. 1(b)]. We see that below a stress of ~5 Pa the shear rate is very small but starts to increase beyond 5 Pa. Thus, below 5 Pa stress, the sample is in a jammed state which acts like a soft solid under small perturbations. The solid line in Fig. 1(c) marks the approximate boundary separating the jammed state and the rejuvenated state. We also carried out a frequency sweep measurement on the jammed steady state as shown in Fig. 1(d) by applying a sinusoidal stress of amplitude 1 Pa. Over the entire frequency range, elastic modulus G' remains larger than viscous modulus G'' signifying the solidlike behavior of the jammed state. The crossover frequency is <0.008 rad/s, implying that the relaxation time is >120 s. The main focus of this Letter is in the region of jamming for CTAT 39 wt%. For an applied stress of 2 Pa, the sample goes into a stress-induced jamming phase after initial aging for ~60 s [Fig. 1(a)]. The nature of the shear-rate fluctuations when the jammed state is fully reached is shown in Fig. 1(b), which shows an almost equal number of positive and negative values. In the steady state, the average shear rate is $\langle\dot{\gamma}\rangle = 3.66 \times 10^{-5}$ s^{-1}. The range of fluctuations is much higher than the instrument resolu-

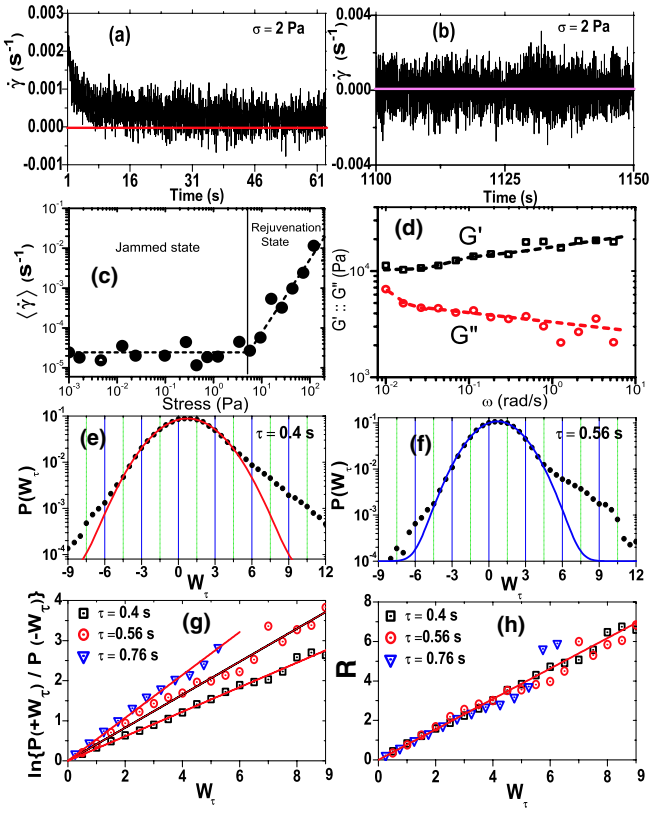

FIG. 1 (color online). (a) The initial aging part for CTAT 39 wt% for the applied stress $\sigma = 2$ Pa. (b) Typical shear-rate fluctuations for CTAT 39 wt% for $\sigma = 2$ Pa. (c) Average shear rate ($\langle\dot{\gamma}\rangle$) vs stress ($\sigma$). (d) Storage ($G'$) and loss ($G''$) modulus vs angular frequency for a CTAT 39 wt% sample (stress amplitude = 1 Pa). The dashed lines are a guide to the eye. Probability distribution functions of W_τ for (e) $\tau = 0.4$ s and (f) $\tau = 0.56$ s, which deviate strongly from Gaussian nature as seen from the Gaussian fits (solid lines). (g) Plot of $\ln[P(+W_\tau)/P(-W_\tau)]$ vs W_τ for different τ's: 0.4, 0.56, and 0.76 s against W_τ; solid lines are the straight line fits to the data. (h) Plot of $R = \frac{1}{\tau}\ln[P(+W_\tau)/P(-W_\tau)]$ vs W_τ for different τ's: 0.4, 0.56, and 0.76 s. Here all of the curves scale into a straight line passing through the origin, as shown by the fitted solid line.

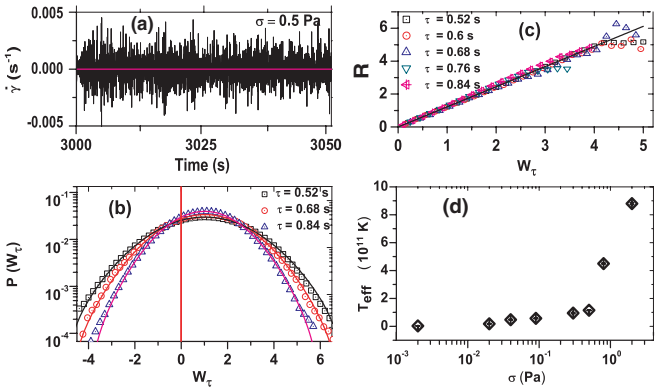

FIG. 2 (color online). (a) Typical shear-rate fluctuations for CTAT 39 wt% for $\sigma = 0.5$ Pa. (b) Probability distribution functions $P(W_\tau)$ vs W_τ. The solid lines are the fits to the Gaussian function. (c) $R = \frac{1}{\tau}\ln[P(+W_\tau)/P(-W_\tau)]$ vs W_τ for different τ's: 0.52, 0.6, 0.68, 0.76, and 0.84 s. All of the curves scale into a straight line passing through the origin, shown by the fitted solid line. (d) T_{eff} vs applied stress σ.

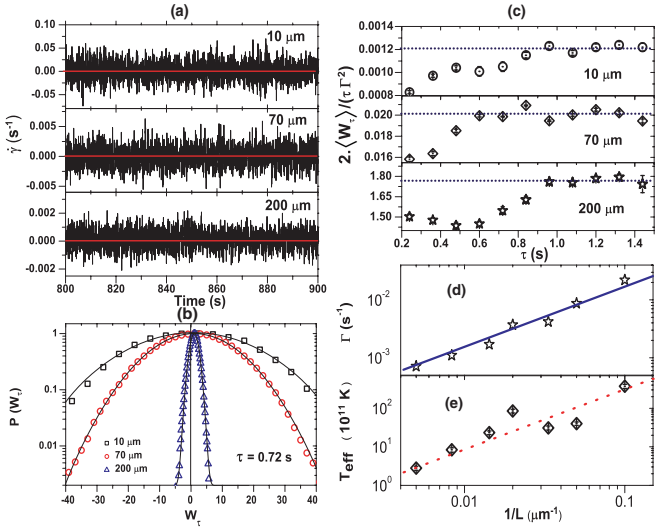

FIG. 3 (color online). (a) The time dependence of $\dot{\gamma}$ for different gaps L between the parallel plates ($L = 10$, 70, and 200 μm) for CTAT 39 wt%. (b) Probability distribution functions of W_τ for $\tau = 0.72$ s for $L = 10$, 70, and 200 μm. The solid lines are fits to the Gaussian function. (c) $2\langle W_\tau\rangle/\tau\Gamma^2$ vs τ. The dotted lines indicate the asymptotic convergence of the function for large τ. (d) Standard deviation Γ of shear-rate fluctuations as a function of $1/L$. The solid line corresponds to $\Gamma \propto 1/L$. (e) Effective temperature (T_{eff}) as a function of $1/L$. The error bars are less than the size of the symbol. The dotted line is a guide to eye.

tion [21]. The global power flux at time t from the rheometer drive to the system $P(t) = \sigma\dot{\gamma}(t)V_s$, where V_s is the volume of the sample. We define a normalized variable $W(t) = s(t)/\langle s(t)\rangle = \dot{\gamma}/\langle\dot{\gamma}\rangle$ and $W_\tau = \frac{1}{\tau}\int_t^{t+\tau} W(t')dt'$. Obviously, $W_\tau = s_\tau/\langle s(t)\rangle$, where $\langle s(t)\rangle = \sigma\langle\dot{\gamma}\rangle V_s/k_B T_{\text{eff}}$ and $\langle\dot{\gamma}\rangle$ is the time-averaged value of shear rate in the steady state over the entire run time. By taking $\Sigma = 1$ as in Ref. [15], Eq. (1) can be simply written in terms of a normalized variable in the large τ limit as

$$R = \frac{1}{\tau}\ln\left[\frac{P(+s_\tau)}{P(-s_\tau)}\right] = \frac{1}{\tau}\ln\left[\frac{P(+W_\tau)}{P(-W_\tau)}\right] = s_\tau = W_\tau\langle s(t)\rangle. \tag{2}$$

Using time-series analysis, we see that the data [Fig. 1(b)] do not correspond to low-dimensional chaos [22]. From these fluctuations in the shear rate, we construct a W_τ time series. At this point, we want to make a brief comment on the averaging procedure. In constructing the W_τ time series, we divided the $s(t)$ series into different bins of length τ. To improve statistical accuracy, we have also taken overlapping bins. To ensure independent sampling, the center of each bin is shifted from the previous one by a time difference (0.12 s) larger compared to the correlation time, which is ≤ 0.04 s. The PDF is the same as obtained by nonoverlapping bins but with higher statistical accuracy. The PDFs for W_τ are strongly non-Gaussian for an integrated power flux for all τ's. We have shown the PDFs for $\tau = 0.4$ s [Fig. 1(e)] and $\tau = 0.56$ s [Fig. 1(f)], and the solid lines correspond to Gaussian fits to the data. In both cases, PDFs show strong deviations from Gaussian nature for $|W_\tau| > 5$, but the quantity $\ln[P(+W_\tau)/P(-W_\tau)]$ goes linearly with W_τ, up to $W_\tau \sim 9$ as shown in Fig. 1(g). The result is nontrivial and corresponds to almost 1 order of magnitude variations in PDFs. Figure 1(h) shows a plot of R vs W_τ where all of the curves scale into a single master curve, a straight line passing through the origin, thus agreeing with Eq. (2). The corresponding slope gives $\langle s(t)\rangle = 0.8 \pm 0.006$ s^{-1}, which corresponds to an effective temperature $T_{\text{eff}} = (8.8 \pm 0.07) \times 10^{11}$ K.

We will now present the result for CTAT 39 wt%, when the applied stress is reduced to 0.5 Pa as shown in Fig. 2. The experiments are done on fresh samples from the same batch of CTAT (39 wt%). In this case, the sample goes to a stress-induced jamming state as soon as the experiment is started. The average shear rate for the steady jammed state is $\langle\dot{\gamma}\rangle = 3.77 \times 10^{-5}$ s^{-1}, which within experimental errors is the same as for 2 Pa stress. The typical nature of shear-rate fluctuations in the jammed state is shown in Fig. 2(a). In this case, the PDFs $P(W_\tau)$ of W_τ [Fig. 2(b)] are perfectly Gaussian for all τ's (only three are shown in the figure for clarity), as depicted by the Gaussian fits in the figure almost over 3 orders of magnitude. From these PDFs, we again estimate the quantity R for different τ's and plot them against W_τ, as shown in Fig. 2(c). All of the curves again scale into a straight line passing through the origin. The magnitude of the slope of the straight line gives $\langle s(t)\rangle = 1.2 \pm 0.0032$ s^{-1}, which gives $T_{\text{eff}} = (1.5 \pm 0.004) \times 10^{11}$ K. We have determined T_{eff} for eight different values of the applied shear stress (σ), shown in a log-linear plot [Fig. 2(d)]. It can be seen that T_{eff} increases with σ, similar to the variation of effective temperature with respect to shear rate in Ref. [23]. We have done experiments for a few more concentrations of CTAT. For samples with a concentration of 35 wt%, the nature of the PDFs for W_τ remains non-Gaussian for a stress level of more than 0.5 Pa. The non-Gaussian fluctuations of W_τ are observed at higher stress values as the surfactant concentration is increased.

We will now turn our attention to the system size dependence of the nature of the observed fluctuations. For this purpose, we have used PP as mentioned earlier, because in CP there is a limit to study system size dependence (when the tip of the cone touches the plate, but still an appreciable amount of sample remains in between). This problem can be overcome by using PP where the gap between the plates can be reduced to an arbitrarily small value. We are aware that PP is not ideal for rheological measurements since, in this geometry, the shear rate increases linearly with the radial distance from the center of the plate (which is compensated in CP by adjusting the angle of the cone). We will, therefore, get an effective value of the shear rate. Since we are interested at this point not in the absolute values of the shear rate but rather in the statistical properties of fluctuations in $\dot{\gamma}$, we will sidestep

this issue. The experiments were done for a 39 wt% sample for the applied stress of 0.5 Pa, with seven gap thicknesses varying between 10 and 200 μm. The nature of fluctuations in $\dot{\gamma}$ is shown in Fig. 3(a) for three values of gap thickness. It can be seen that the amplitude of fluctuations increases as the gap is reduced. Consequently, the width of distributions of W_τ also increases. For each gap, the probability distribution function of W_τ (only for 0.72 s) is shown in Fig. 3(b), for clarity. The PDFs are Gaussian for all τ's in all three cases. This is shown by the fit of the data to the Gaussian function $P(W_\tau) = 1/\sqrt{2\pi\Gamma^2}e^{-(W_\tau-\langle W_\tau\rangle)^2/2\Gamma^2}$, where $\langle W_\tau\rangle$ and Γ^2 are, respectively, the mean and variance of the PDFs of W_τ. Here the Gaussian nature of fluctuations enables us to estimate the ratio of probabilities directly, namely, $\ln[P(+W_\tau)/P(-W_\tau)] = (2\langle W_\tau\rangle/\Gamma^2)W_\tau$. Thus, symmetry like SSFR requires the quantity $1/W_\tau\{\ln[P(+W_\tau)/P(-W_\tau)]\} = (2\langle W_\tau\rangle/\Gamma^2)$ to be a linear function of τ. We have estimated the quantity $(2\langle W_\tau\rangle/\tau\Gamma^2)$ for different τ's from Gaussian fits and plotted them against τ, for three different gap thicknesses, as shown in Fig. 3(c). In all cases we get straight lines parallel to the τ axis [Fig. 3(c)] in the large τ limit, as predicted by SSFR. The effective temperature T_{eff}, estimated from Eq. (2) for different gap values (L), is shown in Fig. 3(e). In calculating T_{eff}, we need a value of the sample volume V_s which is estimated from the geometry of the shear cell. In practice, a small volume of the sample can protrude out of the shear cell which will add error bars in T_{eff}, especially for small L. This error is not possible to estimate accurately. It can be seen that T_{eff} increases as L decreases. The dotted line is a guide to the eye. Further, the standard deviation (Γ) of the shear-rate fluctuations shown in Fig. 3(d) increases as L decreases. The solid line corresponds to $\Gamma \propto 1/L$.

In conclusion, we have shown the evidence of a fluctuation relation in a sheared micellar gel in the jammed state. The system under study is a macroscopically large system which is expected to display "entropy-consuming" fluctuations if the dynamics is determined by long-lived temporal and spatial correlations [16,18]. These long-lived correlations will be present in the jammed state. A physical picture of observing negative shear-rate fluctuations is that a rearrangement in the jammed state can result in feeding the elastic energy from the system to the rheometer drive, resulting in negative $\dot{\gamma}$ fluctuations. Remarkably, we could control the nature of PDF (Gaussian or non-Gaussian) for the same system with applied stress as a tunable parameter. The symmetry properties of the PDFs like SSFR is verified in the nontrivial case of non-Gaussian fluctuations with good statistical accuracy, due to a huge number of large negative fluctuations. We show that an effective temperature of the jammed state can be defined experimentally using FR. It will be interesting to explore the connection between our results and a recent theoretical work on defining the temperature of a static granular assembly [24]. Our observations open up a possibility of formulation of statistical mechanics of a driven jammed state in an equivalent stress ensemble. Our preliminary experiments on other systems such as clay suspensions showing a jammed state suggest that the nonequilibrium fluctuations in viscosity, both positive and negative, are generic features of a jammed state. We hope that our experimental observations will stimulate many new experiments and theories on nonequilibrium fluctuations in macroscopic systems.

A. K. S. acknowledges the Council of Scientific and Industrial research (CSIR) of the Government of India for financial support.

*asood@physics.iisc.ernet.in

[1] D. J. Evans, E. D. G. Cohen, and G. P. Morris, Phys. Rev. Lett. **71**, 2401 (1993).
[2] D. J. Evans and D. J. Searles, Phys. Rev. E **50**, 1645 (1994).
[3] G. Gallavotti and E. D. G. Cohen, Phys. Rev. Lett. **74**, 2694 (1995); G. Gallavotti and E. D. G. Cohen, J. Stat. Phys. **80**, 931 (1995).
[4] R. van Zon and E. G. D. Cohen, Phys. Rev. Lett. **91**, 110601 (2003).
[5] D. M. Carberry *et al.*, Phys. Rev. Lett. **92**, 140601 (2004).
[6] G. M. Wang *et al.*, Phys. Rev. Lett. **89**, 050601 (2002).
[7] N. Garnier and S. Ciliberto, Phys. Rev. E **71**, 060101 (2005).
[8] D. Collin *et al.*, Nature (London) **437**, 231 (2005).
[9] J. Liphardt *et al.*, Science **296**, 1832 (2002).
[10] F. Douarche, S. Ciliberto, and A. Petrosyan, J. Stat. Mech. (2005) P09011.
[11] F. Douarche *et al.*, Phys. Rev. Lett. **97**, 140603 (2006).
[12] X. D. Shang, P. Tong, and K. Q. Xia, Phys. Rev. E **72**, 015301 (2005).
[13] S. Ciliberto and C. Laroche, J. Phys. IV (France) **8**, Pr6-215 (1998).
[14] S. Ciliberto *et al.*, Physica (Amsterdam) **340A**, 240 (2004).
[15] K. Feitosa and N. Menon, Phys. Rev. Lett. **92**, 164301 (2004).
[16] M. M. Bandi *et al.*, arXiv:nlin.CD/0607037v2, and references therein.
[17] W. I. Goldburg *et al.*, Phys. Rev. Lett. **87**, 245502 (2001).
[18] G. Gallavotti, Eur. Phys. J. B **61**, 1 (2008).
[19] J. F. A. Soltero and J. E. Puig, Langmuir **11**, 3337 (1995).
[20] P. Coussot *et al.*, J. Rheol. (N.Y.) **46**, 573 (2002).
[21] A typical shear-rate fluctuation of 0.001 s^{-1} observed in our experiments and a sample time of 40 ms imply a shear deformation $\gamma = 4 \times 10^{-5}$. This corresponds to an angular displacement $\phi = \gamma\times$ cone angle $(\beta) = 1.4$ μrad, which is much larger than the angular resolution of the instrument (0.01 μrad), which can be found in the technical specifications of the MCR300 rheometer at the site http://www.oleinitec.fi/pdf/Physica/mcr-serie-e.pdf.
[22] R. Ganapathy *et al.*, Phys. Rev. Lett. **96**, 108301 (2006); R. Bandyopadhyay *et al.*, *ibid.* **84**, 2022 (2000).
[23] I. K. Ono *et al.*, Phys. Rev. Lett. **89**, 095703 (2002).
[24] S. Henkes *et al.*, Phys. Rev. Lett. **99**, 038002 (2007).